atmosphere

MDPI

Article

Retrieval of Plateau Lake Water Surface Temperature from UAV Thermal Infrared Data

Ouyang Sima [1,2], Bo-Hui Tang [1,2,3,*], Zhi-Wei He [1,2], Dong Wang [1,2] and Jun-Li Zhao [1,2]

[1] Faculty of Land Resource Engineering, Kunming University of Science and Technology, Kunming 650093, China; ou-yangsyma@stu.kust.edu.cn (O.S.); hezw@stu.kust.edu.cn (Z.-W.H.); wangdong@stu.kust.edu.cn (D.W.); zhaojl@stu.kust.edu.cn (J.-L.Z.)
[2] Key Laboratory of Plateau Remote Sensing, Department of Education of Yunnan Province, Kunming 650093, China
[3] State Key Laboratory of Resources and Environmental Information System, Institute of Geographic Sciences and Natural Resources Research, Chinese Academy of Sciences, Beijing 100101, China
* Correspondence: tangbh@kust.edu.cn

Abstract: The lake water surface temperature (LWST) is a critical parameter influencing lake ecosystem dynamics and addressing challenges posed by climate change. Traditional point measurement techniques exhibit limitations in providing comprehensive LWST data. However, the emergence of satellite remote sensing and unmanned aerial vehicle (UAV) Thermal Infrared (TIR) technology has opened new possibilities. This study presents an approach for retrieving plateau lake LWST (p-LWST) from UAV TIR data. The UAV TIR dataset, obtained from the DJI Zenmuse H20T sensor, was stitched together to form an image of brightness temperature (BT). Atmospheric parameters for atmospheric correction were acquired by combining the UAV dataset with the ERA5 reanalysis data and MODTRAN5.2. Lake Water Surface Emissivity (LWSE) spectral curves were derived using 102 hand-portable FT-IR spectrometer (102F) measurements, along with the sensor's spectral response function, to obtain the corresponding LWSE. Using estimated atmospheric parameters, LWSE, and UAV BT, the un-calibrated LWST was calculated through the TIR radiative transfer model. To validate the LWST retrieval accuracy, the FLIR Infrared Thermal Imager T610 and the Fluke 51-II contact thermometer were utilized to estimate on-point LWST. This on-point data was employed for cross-calibration and verification. In the study area, the p-LWST method retrieved LWST ranging from 288 K to 295 K over Erhai Lake in the plateau region, with a final retrieval accuracy of 0.89 K. Results demonstrate that the proposed p-LWST method is effective for LWST retrieval, offering technical and theoretical support for monitoring climate change in plateau lakes.

Keywords: unmanned aerial vehicle (UAV); plateau lakes; lake water surface temperature (LWST); lake water surface emissivity (LWSE); radiative transfer model

Citation: Sima, O.; Tang, B.-H.; He, Z.-W.; Wang, D.; Zhao, J.-L. Retrieval of Plateau Lake Water Surface Temperature from UAV Thermal Infrared Data. *Atmosphere* **2024**, *15*, 99. https://doi.org/10.3390/atmos15010099

Academic Editor: Graziano Coppa

Received: 7 December 2023
Revised: 9 January 2024
Accepted: 10 January 2024
Published: 12 January 2024

1. Introduction

Lake water surface temperature (LWST) plays a pivotal role in shaping local climate and hydrological processes, standing as a fundamental parameter within lake ecosystems [1]. The investigation of LWST holds significant importance in elucidating the operational dynamics of lake ecosystems and addressing the challenges presented by climate change and extreme weather events [2]. Lakes, as indispensable freshwater reservoirs on Earth, support diverse ecosystems. The quality and temperature of water in lakes are crucial determinants of biodiversity and ecological equilibrium. With the intensification of climate change, lake ecosystems encounter unprecedented stressors. Given water's notable heat capacity, even slight fluctuations in lake water surface temperature can notably influence overall water quality and the functionality of ecosystems. The global temperature elevation has resulted in heightened lake temperatures, posing a threat to lake ecosystems. The warming of lakes may instigate shifts in water circulation patterns, uneven dispersion

of oxygen, and an escalation in cyanobacterial blooms, thereby jeopardizing aquatic life [3]. However, the ramifications of elevated LWST on lake aquatic ecosystems are intricate and multifaceted. Hence, real-time and precise monitoring of temporal and spatial fluctuations and distributions of LWST stands as a critical necessity. Therefore, the acquisition of high spatiotemporal resolution LWST data for lakes holds paramount significance.

Given the complexity of inferring LWST, conventional point measurement techniques in the field struggle to provide accurate and comprehensive LWST coverage over large areas efficiently. Fortunately, satellite remote sensing data can retrieve Land Surface Temperature (LST) with high precision, offering ample temporal resolution and complete spatial coverage, transcending the limitations of singular point measurements [4]. LST holds significant utility across a spectrum of domains, spanning from the monitoring of mountainous ecosystems, the analysis of crop growth patterns, the assessment of hydrological cycles, the surveillance and management of forests, environmental conservation and monitoring, and the estimation of evapotranspiration. Over the years, multiple algorithms have been developed to infer LST from satellite Thermal Infrared (TIR) data, typically within the 8–14 μm range [5]. These algorithms include the Single Channel (SC) algorithm [6,7], Split Window (SW) algorithm [8–13], Temperature Emissivity Separation (TES) algorithm [14,15], Day-Night (DN) algorithm [16], and Dual-Angle (DA) algorithm [17]. However, it is crucial to acknowledge that satellite imagery is vulnerable to cloud interference, leading to temporal disruptions in available data. Additionally, the current spatial resolution of available satellite TIR data is generally low [18], potentially insufficient to meet the demand for real-time, precise monitoring of LWST spatiotemporal variations and attribution analysis. [19].

In recent years, the utilization of unmanned aerial vehicle (UAV) TIR remote sensing has gained substantial traction, capitalizing on its advantages of high spatial resolution and resilience to cloud interference. This technology has found widespread application, notably in temperature retrieval [20–23]. Numerous studies have explored the potential of UAV TIR data for retrieving LST. For instance, Awais et al. employed the DJI M300 RTK UAV equipped with the DJI Zenmuse XT2 TIR camera to capture TIR images. They converted grayscale values directly into LST, validating the retrieved temperatures using contact thermometers [24]. Naughton et al., utilizing the DJI M100 UAV paired with the DJI Zenmuse XTR TIR camera, obtained high-resolution LST in their study area, assessing daily variations and uncertainties in LST [25]. Heinemann et al. concentrated on agricultural areas and proposed an LST retrieval algorithm by integrating multispectral and UAV TIR remote sensing images along with NDVI thresholds [26]. Some studies have ventured into utilizing UAVs for research on LWST. For instance, Xu et al. employed UAVs for continuous daytime and nighttime observations of urban LST, analyzing thermal runoff pollution and its subsequent impact on LWST [27]. However, none of the aforementioned methodologies directly and independently retrieved the temperatures of large water bodies. This underscores the existing gap in utilizing UAV TIR data for the direct retrieval of LWST, particularly in the context of plateau LWST retrieval. The method proposed in this paper can serve as a reference for UAV TIR retrieval studies of plateau LWST and provide technical support for monitoring changes in LWST and attributive analysis.

Based on this, we propose a method for remote sensing retrieval of plateau lake water surface temperature (p-LWST). The main steps of the p-LWST method are as follows:

(a) Employing an UAV equipped with a TIR camera to acquire TIR data.

(b) Utilizing ERA5 reanalysis data and MODTRAN5.2 to estimate atmospheric parameters in the study area for atmospheric correction.

(c) Determining lake water surface emissivity (LWSE) spectral curves by using 102 hand portable FT-IR spectrometer (102F) measurements combined with the sensor's spectral response function to obtain the corresponding LWSE.

(d) Employing the FLIR T610 infrared thermal imaging camera to obtain on-point LWST, performing cross-calibration of the surface temperature obtained by the UAV, and ultimately retrieving LWST.

2. Materials

2.1. Study Area

This study focuses on a typical plateau lake, Erhai Lake, situated in Dali City, Dali Bai Autonomous Prefecture, Yunnan Province, China (Figure 1). Erhai Lake is located between 99°58′ and 100°27′ E longitude and 25°25′ and 25°58′ N latitude. It falls within the North Subtropical Plateau Monsoon Climate Zone, characterized by minimal annual temperature fluctuations and indistinct seasonal variation.

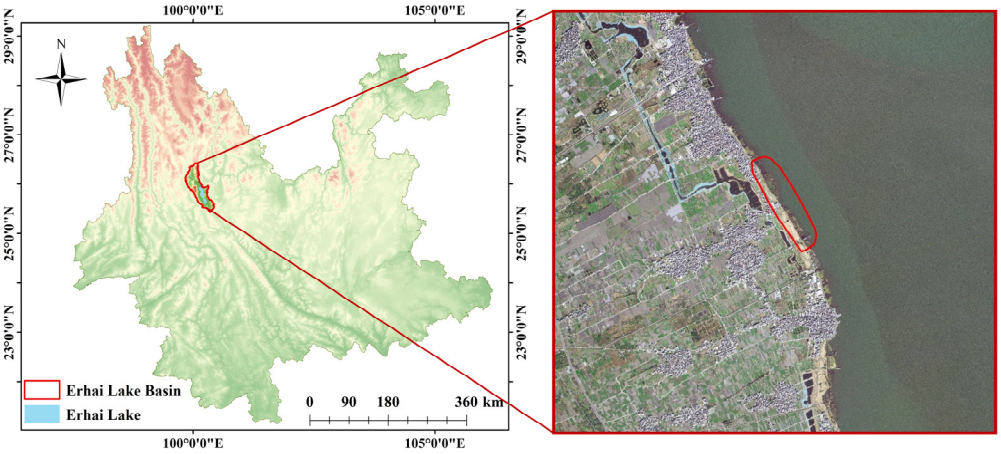

Figure 1. Study area (the area enclosed in the red box in the right picture is the study area).

2.2. Air-Ground Synchronization Experiment

By designing an air-ground synchronization experiment, TIR data from the UAV, measured LWST, and measured LWSE data were simultaneously obtained. It is assumed that overall changes in LWST and LWSE are negligible during the UAV flight process.

The experiment consists of two parts: (1) UAV TIR imaging and (2) random measurements of LWSE and LWST. The air-ground synchronization experiment was conducted on 4 November 2023, between 10:30 and 11:30 in the morning. The UAV operated at an altitude of 300 m, maintaining a speed of 8 m/s, with a 90% heading overlap, and a 90% side overlap. The flight route is a total of 12,684 m long, covering an aggregate area of 204,313 m^2. These parameters were meticulously chosen to ensure substantial image overlap critical for subsequent orthomosaic image integration. The weather conditions on that day were characterized by clear skies and minimal cloud cover. Solar radiance was pronounced during this period, contributing to the relatively elevated LWST. In conjunction with the TIR imaging by the UAV, 102F was concurrently deployed on a ship for random measurements of the LWSE (Figure 2a). The synchronized lake imaging was conducted for cross-calibration purposes using the FLIR T610 infrared thermal imaging camera (Figure 2b) and the Fluke 51-II contact thermometer (Figure 2c). The focus of this study lies in water surface temperature rather than direct water body temperature assessment. Hence, the accuracy validation was performed using the FLIR T610 infrared thermal imaging camera. The final inversion-derived LWST results can be validated by comparing them with the LWST results obtained from T610. This comparison serves to verify the accuracy of the research methodology employed.

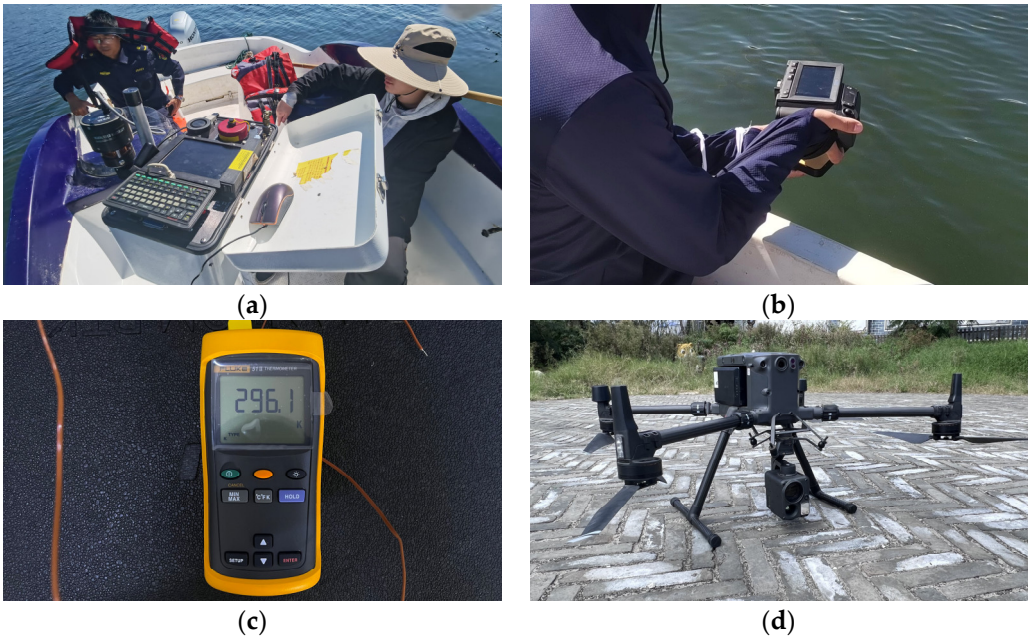

Figure 2. Air-ground synchronization experiment. (**a**) 102F for measuring LWSE, (**b**) T610 for measuring LWST, (**c**) Fluke 51-II contact thermometer, (**d**) DJI M300 RTK UAV equipped with a DJI Zenmuse H20T TIR camera.

In this study, the Root Mean Square Error (RMSE) is employed as a metric to gauge the disparity between the inverted results and actual values. A smaller RMSE value indicates a superior fidelity of the inverted results to the ground truth.

The experiment utilized a DJI M300 RTK UAV equipped with a DJI Zenmuse H20T camera (both from DJI, China) to capture TIR data (Figure 2d). The DJI Zenmuse H20T camera, produced by DJI, is a multifunctional camera that integrates four types of sensors. It includes a TIR sensor, two visible light sensors, and a laser rangefinder. The TIR sensor has an image resolution of 640 × 512 pixels, a pixel pitch of 12 µm, a wavelength range of 8 to 14 µm, a temperature measurement range of −40 °C to 150 °C, an accuracy of ±2 °C, and a sensitivity of <0.05 °C.

The 102F is manufactured by Designs and Prototypes company (USA). It is designed for measuring the radiance or emissivity of the Earth's surface and calibrating atmospheric effects for satellites or airborne scanners. The spectral range of 102F spans from 2 to 16 µm, with a spectral accuracy of ±1 cm^{-1}.

The FLIR T610 infrared thermal imaging camera, manufactured by Teledyne FLIR, features a TIR resolution of 640 × 480 pixels, a wavelength range of 7.5 to 14 µm, a temperature measurement range of −40 °C to 150 °C, an accuracy of ±2 °C, and a sensitivity of <0.04 °C.

The Fluke 51-II contact thermometer, produced by Fluke, is a single-channel temperature meter equipped with an 80PK-1 K-type thermocouple probe. It has a temperature measurement range of −200 °C to 1372 °C, with an accuracy of ±[0.05% + 0.3 °C].

2.3. Data Preprocessing

Initially, the TIR images captured by the UAV require processing. These original images, obtained from DJI Zenmuse H20T, are currently in JPG format. The primary objective is to convert each H20T image into TIFF format to facilitate the extraction of brightness temperature information (°C). However, it's crucial to acknowledge the potential loss of geolocation data during this conversion process. To mitigate this, it is recommended to first utilize DJI Terra (v3.9.0) software for the extraction and preservation of geolocation data from the images before proceeding with the conversion from JPG to TIFF format.

It is crucial to emphasize that the quality of mosaic stitching directly affects the subsequent retrieval of LWST. Hence, obtaining clear images and selecting appropriate image stitching methods become pivotal. In this study, we utilized Pix4dMapper (v4.4.12) software to achieve satisfactory mosaic results. Ultimately, we acquired the TIR image brightness temperature data for the entire study area (Figure 3).

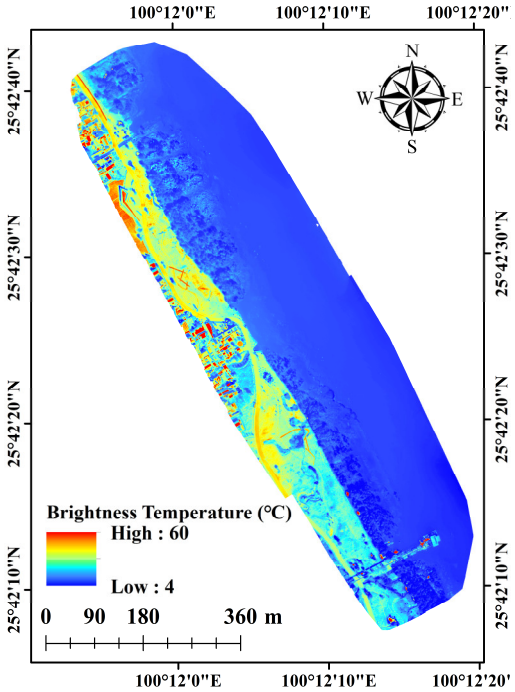

Figure 3. The spatial distribution of brightness temperature data acquired by UAV in the study area.

Previous research findings have consistently highlighted the influence of UAV flight altitude and image overlap rate on the stitching outcome. After conducting multiple UAV flight experiments, it was established that within our study area, setting the UAV's flight altitude in the range of 250 to 300 m, with both heading and side overlap rates set at 85% or higher, consistently yields optimal stitching results.

Figure 3 illustrates that higher temperatures are predominantly concentrated on the ground and in surrounding villages. Overall, the brightness temperatures within the lake area remain relatively low, and no significant outliers are observed within the lake.

3. Methods

3.1. LWST Retrieval Algorithm Based on Radiative Transfer Equation

The TIR radiance received by the UAV sensor primarily consists of three components [4,18]: surface thermal radiance, atmospheric upwelling radiance from the water surface to the flight altitude of the UAV, and atmospheric downwelling radiance from the entire atmospheric column, including the reflection from the water surface, as shown in Figure 4. Therefore, the radiance received by the TIR camera can be succinctly expressed as follows:

$$L_{TOA} = \left[\varepsilon \cdot B(T_S) + (1-\varepsilon)\cdot L^{\downarrow}\right]\cdot\tau + L^{\uparrow} \quad (1)$$

In Equation (1), L represents the radiance at the entrance pupil of the sensor ($W/(m^2 \cdot sr \cdot \mu m)$); τ is the atmospheric transmittance from the water surface to the flight altitude; ε is the emissivity of the water surface; $B(T_s)$ is the blackbody radiance ($W/(m^2 \cdot sr \cdot \mu m)$) corresponding to the surface temperature T_s; $L^{\downarrow}$ and $L^{\uparrow}$ denote the atmospheric downwelling and upwelling radiance ($W/(m^2 \cdot sr \cdot \mu m)$).

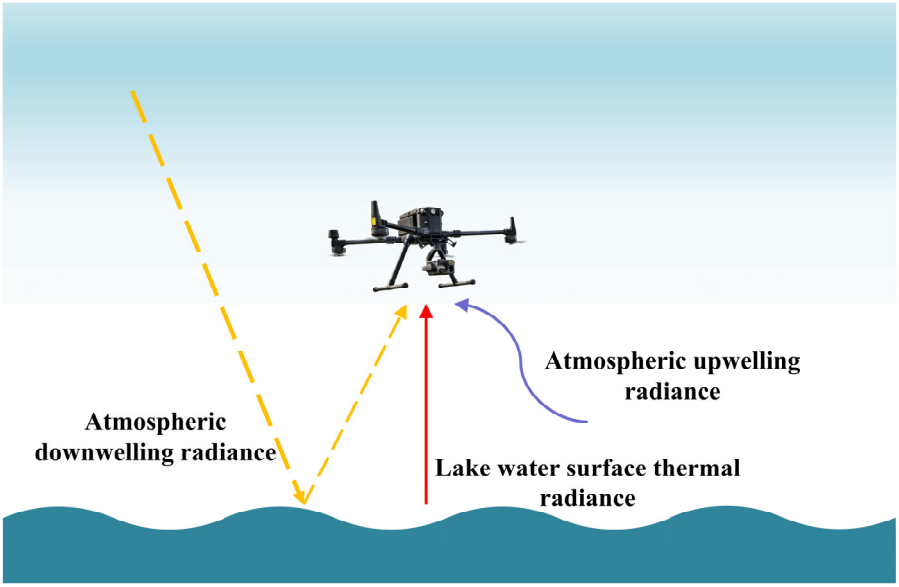

Figure 4. Radiance transmission of UAV TIR imaging.

Based on Equation (1), the blackbody radiance $B(T_s)$ of the water surface temperature T_s can be expressed as follows:

$$B(T_s) = \frac{\left[L_{TOA} - L^{\uparrow} - \tau \cdot (1-\varepsilon) \cdot L^{\downarrow}\right]}{\tau \cdot \varepsilon} \tag{2}$$

According to the experimental values of L, $L^{\uparrow}$, $L^{\downarrow}$, τ, and as obtained using Equation (2), we can calculate $B(T_s)$. Subsequently, by employing the Planck formula retrieval, we can determine the water surface temperature.

$$T_s = k_2 / \left[\lambda \cdot ln\left(1 + \frac{k_1}{\lambda^5 \cdot B(T_s)}\right)\right] \tag{3}$$

In Equation (3), k_1 and k_2 are constants ($k_1 = 1.19104 \times 10^{-16}$ W·m^2 and $k_2 = 1.43877 \times 10^{-2}$ m·K); λ represents the effective wavelength of the sensor's spectral band (λ = 11.0580 μm).

3.2. Atmospheric Correction

The TIR data obtained by the UAV are primarily influenced by three components: surface thermal radiance, atmospheric upwelling radiance from the water surface to the UAV's flight altitude, and downwelling radiance from the entire atmospheric column due to water surface reflection. In order to mitigate their impact on the TIR signals, it is essential to acquire these three parameters initially.

ERA 5, the fifth-generation atmospheric reanalysis produced by the European Centre for Medium-Range Weather Forecasts (ECMWF), currently spans the time period from 1940 to the present day. It provides the requisite atmospheric profiles for atmospheric correction, offering a meteorological dataset of 1-hourly pressure level analyses. This dataset encompasses air temperature, relative humidity, and geopotential height at 37 pressure levels, ranging from 1000 hPa to 1 hPa, with a spatial resolution of 0.25° × 0.25°. These data can be obtained from the ECMWF website (https://cds.climate.copernicus.eu/ (accessed on 10 November 2023)).

The Moderate Resolution Atmospheric Transmission model (MODTRAN5.2) [28] was utilized to simulate the atmospheric transmission process and calculate atmospheric parameters for TIR imaging from an UAV. Atmospheric profile data for the corresponding time (morning of 4 November 2023, from 10:30 to 11:30) were obtained from ERA5 reanalysis data. Subsequently, MODTRAN5.2 was employed to calculate the entire atmospheric down-

welling radiance. By convolving the spectral response functions of the DJI Zenmuse TIR lens with simulated data from MODTRAN5.2, one can derive the atmospheric upwelling radiance, atmospheric downwelling radiance, and atmospheric transmittance across the entire spectrum.

3.3. Estimation of LWSE

The 102F serves as the primary tool in this study, operating based on the following principles: Infrared radiation emitted by the target under examination is initially directed through a sampling lens into the spectrometer. Subsequently, the radiation undergoes spectral analysis via Fourier transformation. The spectrally resolved radiation is then directed to a detector for reception, enabling precise determination of the target's emissivity. This advanced spectral analysis technique provides a highly sensitive and accurate means for investigating the emissivity of various components within water bodies.

Due to the focus of this study on water body analysis, the emissivity of the study area's waters was determined using 102F. To acquire a more comprehensive dataset, systematic and random emissivity measurements were conducted at various distances from the shoreline. This grid-based sampling approach aids in capturing spatial variations in water properties, thereby providing a more detailed foundational dataset for subsequent analyses.

In the nearshore waters, there is a substantial presence of aquatic plants, such as the Ottelia (Figure 5a). To comprehensively understand the impact of water lilies on the emissivity of the water body, emissivity measurements were conducted in both the water areas covered by water lilies and the deeper regions. Figure 5b illustrates the emissivity spectral curves obtained from these two categories of water areas, revealing slight discrepancies with minimal variations observed. By convolving the measured emissivity spectral curves with the spectral response function of the sensor, emissivity values were derived, and their average was taken as the emissivity for the lake surface.

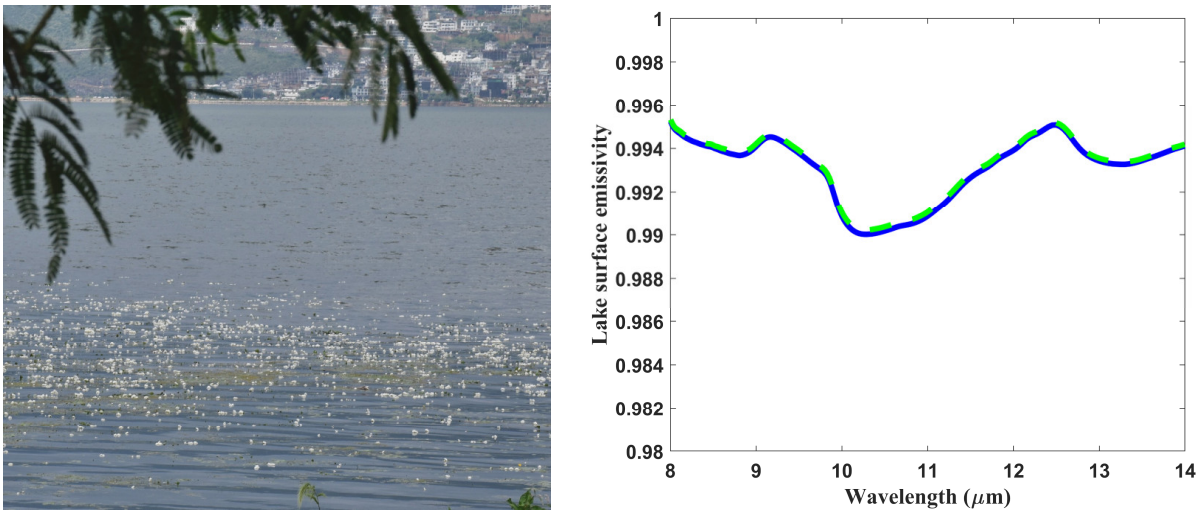

Figure 5. (**a**) Aquatic plants in the study area (Ottelia), (**b**) The emissivity of the water body measured by using the 102F (the blue solid line and the green dashed line represent the LWSE measured at different locations).

3.4. Cross-Calibration

The brightness temperature data captured by the equipped TIR lens requires calibration. This study employs the FLIR T610 infrared thermal imaging camera and the Fluke

51-II contact thermometer to cross-calibrate the remotely sensed LWST from the UAV, enhancing the precision of the inferred LWST.

$$L_g = \varepsilon_g B\left(T_{s_g}\right) + \left(1 - \varepsilon_g\right) R_{environment} \tag{4}$$

$$L_w = \varepsilon B(T_{s_w}) + (1 - \varepsilon) R_{environment} \tag{5}$$

In the equation, L_g and L_w represent the radiance (W/(m^2·sr·μm)) measured from the golden plate and water body, respectively. ε_g denotes the emissivity of the golden plate (ε_g = 0.04). $B(T_{Sg})$ and $B(T_{Sw})$ stand for the blackbody radiance (W/(m^2·sr·μm)) corresponding to the temperature of the golden plate (T_{Sg}) and the measured water temperature (T_{Sw}). $R_{environment}$ accounts for the environmental radiance. T_{Sg} is known from the Fluke 51-II contact thermometer. $B(T_{Sg})$ can be determined by using the Planck formula.

Based on Equation (4), the environmental radiance $R_{environment}$ can be expressed as:

$$R_{environment} = \frac{L_g - \varepsilon_g B\left(T_{s_g}\right)}{\left(1 - \varepsilon_g\right)} \tag{6}$$

Based on the determined values of L_g, ε_g, and the computed $B(T_{Sg})$, the environmental radiance can be calculated. Assuming a constant environmental radiance, given the measured L_w, ε, and the computed $R_{environment}$, the Plank formula allows for the derivation of $B(T_{Sw})$.

$$B(T_{s_w}) = \frac{L_w - (1 - \varepsilon) R_{environment}}{\varepsilon} \tag{7}$$

Based on the derived $B(T_{Sw})$, the LWST obtained from the FLIR infrared thermal imager T610 can be determined according to Equation (3). Random sampling within the study area theoretically suggests that the LWST retrieved from T610 is higher compared to the LWST retrieved from UAV TIR data. Therefore, the cross-calibration Equation can be expressed as:

$$\delta Ts = \frac{1}{N} \sum_{k=1}^{N} \left(T_{s_{w,k}} - T_{s_k}\right) \tag{8}$$

In the Equation, N represents the total number of sampling points. After obtaining δT_S, the final calculation Equation for LWST is determined as follows:

$$LWST = T_S + \delta Ts \tag{9}$$

3.5. Retrieval Accuracy Verification of LWST

In this study, the actual LWST measured by the FLIR infrared camera T610 was used to verify the accuracy of the retrieved LWST by the p-LWST method. The actual LWST was measured randomly on the surface of lakes in the study area and then compared with the retrieval LWST obtained by the p-LWST method. The retrieval error calculation formula can be expressed as follows:

$$RMSE = \left[\frac{1}{N} \sum_{k=1}^{N} \left(T_{s_{w,k}} - T_{s_k}\right)^2\right]^{1/2} \tag{10}$$

where the RMSE is the root-mean-squared error.

4. Results

4.1. Results Analysis of LWST Retrieved by the p-LWST Method

The data regarding atmospheric upwelling radiance, atmospheric downwelling radiance, and atmospheric transmittance for the study area were acquired using MODTRAN5.2 (Table 1). The LWSE, measured by 102F, is ε = 0.993. The focus of this study is the water

body, yet the thermal imaging via UAV encompasses land areas. Consequently, a masking procedure was applied to the land sections, which are disregarded during the retrieval process, ensuring a dedicated focus on retrieving LWST.

Table 1. Calculated atmospheric parameters using MODTRAN5.2.

Height m	Atmospheric Upwelling Radiance W/(m^2·sr·μm)	Atmospheric Downwelling Radiance W/(m^2·sr·μm)	Atmospheric Transmittance
300	0.8570	4.8608	0.9035

Through cross-calibration, the LWST of the study area was successfully retrieved, as depicted in Figure 6. The retrieval results indicate that LWST predominantly ranges between 288 K and 295 K, exhibiting pronounced spatial variations. Particularly in nearshore areas, temperatures remain relatively higher, ranging between 292 K and 293 K. In contrast, regions closer to the lake center display lower temperatures, notably in the lower right corner of the study area, where temperatures reach a minimum between 288–290 K. Overall, the majority of the area shows water temperatures concentrated within the range of 290–291.5 K, as illustrated in Figure 7.

The spatial variability in temperature distribution can be influenced by multiple factors. Specifically, higher temperatures observed near shorelines might be associated with the extensive presence of algae blooms and aquatic vegetation in these regions. Furthermore, during the experiment, there was a notably intense direct solar radiance, which exerted a prolonged impact due to extended exposure to sunlight. It is worth noting that our retrieval of LWST closely corresponds to the observed conditions, potentially attributed to an extended duration without cloud cover, resulting in direct solar radiation.

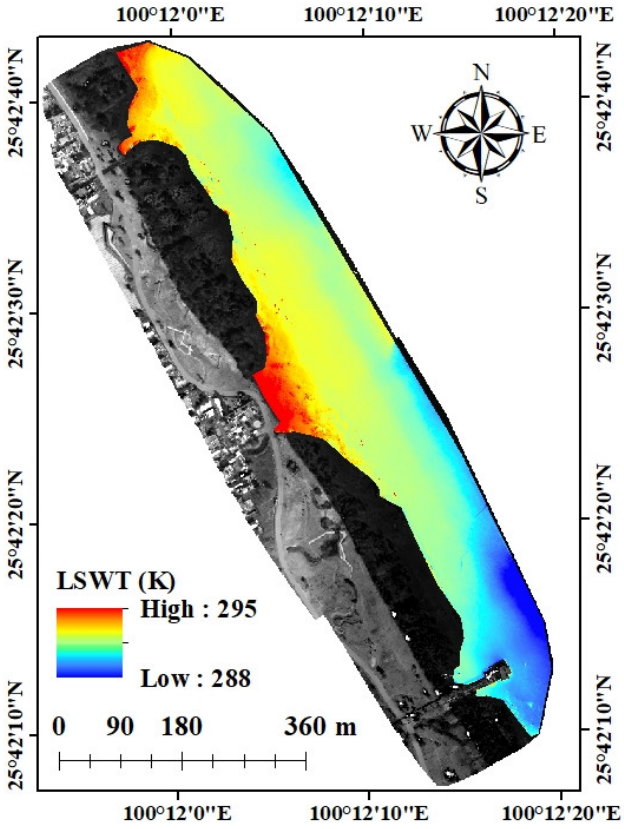

Figure 6. LWST retrieval results (black areas represent land and vegetation).

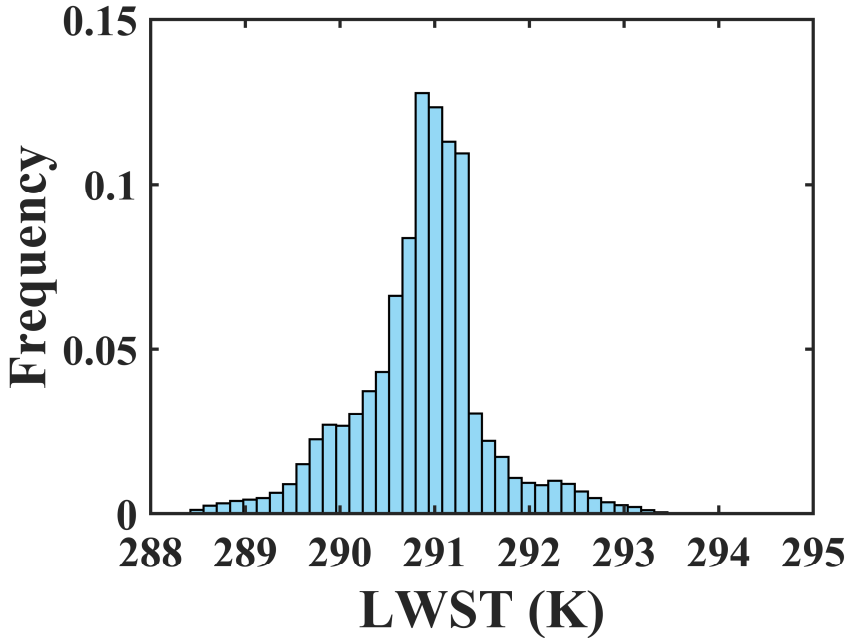

Figure 7. Histogram of the LWST Distribution.

4.2. Accuracy Validation of LWST

In this paper, 20 randomly sampled values obtained by the FLIR T610 infrared thermal imaging camera in the study area were compared with the LWST derived from UAV TIR data (Table 2). As depicted in Figure 8, the RMSE is 0.89 K. This signifies that the proposed methodology achieves a high level of accuracy in LWST retrieval.

Table 2. The LWST from T610 and the p-LWST method, respectively.

Code	LWST from T610	LWST from the p-LWST Method	Bias
1	291.06	291.35	0.29
2	291.99	291.29	−0.70
3	291.52	291.28	−0.24
4	291.30	291.22	−0.08
5	291.38	291.00	−0.39
6	291.36	291.04	−0.33
7	291.72	290.91	−0.81
8	290.20	291.05	0.85
9	290.42	289.99	−0.43
10	290.22	290.20	−0.02
11	291.73	290.28	−1.45
12	291.33	290.64	−0.69
13	291.03	290.59	−0.44
14	291.14	290.83	−0.31
15	291.04	290.87	−0.17
16	291.34	290.95	−0.39
17	291.04	291.10	0.07
18	290.44	291.65	1.21
19	290.93	292.32	1.39
20	290.64	293.28	2.63

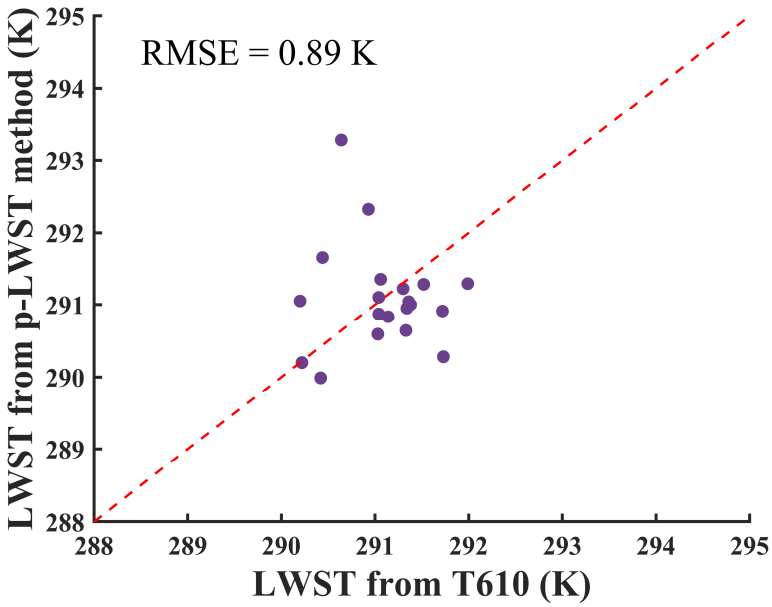

Figure 8. RMSE of the LWST from T610 and the p-LWST method (the purple dots represent 20 key points of LWST, while the red dashed line represents the 1:1 line).

5. Discussion

5.1. The Influence of Flight Altitude on Retrieval Results

During UAV flights, despite operating at a relatively low altitude, the atmospheric conditions significantly impact the signal reception of the TIR camera onboard. Through remote control manipulation, we observed a non-linear trend in the brightness temperature at a specific location corresponding to the increase in UAV flight altitude. Notably, there was a substantial decrease in the brightness temperature of the ground area, ranging from 15 °C to 20 °C, while the water surface experienced losses within the range of 10 °C to 13 °C.

It is noteworthy that prior investigations also employed DJI Zenmuse series TIR lenses, typically constraining UAV flight altitudes to the range of 70 m to 150 m [27]. However, within this altitude range, such a pronounced phenomenon of brightness temperature loss was not evident. Kelly et al. [26] extensively probed this issue and emphasized the TIR camera's susceptibility to internal temperature variations, particularly in low-cost models that often lack radiometric calibration. Common factors influencing UAV flights, such as wind and temperature drift, lead to a non-linear relationship between camera output and sensor temperature. To obtain high-quality stitched images of water surfaces and cover extensive water bodies, we ultimately opted for a UAV flight altitude of 300 m. However, this decision unavoidably magnified the impacts of wind and temperature drift.

Considering the study's practical needs, we selected time periods with lower wind speeds for experimentation and carefully deliberated on flight speed to strike a balance between image quality and the necessary coverage range, aiming to mitigate wind and temperature drift effects. Despite these considerations, temperature drift persisted [29]. Future endeavors may explore suitable temperature-correction algorithms to further refine image quality.

5.2. The Influence of Cross-Calibration on Retrieval Results

To address the issue of brightness temperature loss, we conducted a cross-calibration process on the acquired image brightness temperatures. Based on theoretical feasibility, a correction value (δT_S = 12.82 K) was applied uniformly to all temperature values to ensure that the retrieved LWST fell within a normal range. However, cross-calibration also introduces errors. As this study did not validate the precision of the LWST retrieval, it was assumed that the impact of cross-calibration was relatively minor. In future research en-

deavors, we aim to employ appropriate methodologies for a more comprehensive accuracy assessment of both LWST retrievals and cross-calibration. This effort will aid in evaluating the precise influence of cross-calibration on the final outcomes, thereby enhancing the study's reliability.

5.3. The Influence of UAV Image Stitching on the Retrieval Results

The imagery in this study was stitched using Pix4DMapper (v4.4.12) software, long regarded as the premier choice for UAV image stitching [24]. The primary focus of this research lies on bodies of water, an area where image stitching has historically posed a challenge in photogrammetry. Due to certain issues with flight path configurations, images captured along flight lines near the lake's center solely depict the water body, resulting in an insufficient extraction of feature points during the image registration process, thereby causing stitching failures.

Despite achieving satisfactory final stitching outcomes, uncertainties persist regarding potential information loss in the water body region. Against this backdrop, for a more comprehensive assessment of the accuracy and integrity of the water body area, it is imperative for future endeavors to undertake in-depth analyses and investigations.

5.4. The Influence of Water Body Emissivity on Retrieval Results

While this study randomly determined the emissivity of the water body, it did not achieve a per-pixel determination. Consequently, the final emissivity value of the water body was obtained by averaging the emissivity values of all sampled points. The study did not account for the emissivity of aquatic vegetation, such as Ottelia, within the lake. Considering the widespread coverage of macrophytes in nearshore areas, this absence might impact the retrieval results of the LWST in these nearshore regions. Moreover, as the water depth varies, the lake's central position approximates pure water, inevitably differing in emissivity from the water body in nearshore areas.

5.5. Future Work and Prospects

In regard to this study, there are still areas for improvement. While we consistently underscored the impact of atmospheric radiance on our research, we only considered the atmospheric profile at a UAV's flight altitude, assuming minimal variations in the atmospheric profile below this altitude. To enhance the accuracy of LWST retrieval, future research could contemplate conducting experiments using UAVs at various flight altitudes during the same time frame.

Considering that our study primarily addresses the issue of brightness temperature loss rather than rigorously verifying LWST accuracy, we conducted an initial estimation of the errors introduced by the cross-calibration. In forthcoming research endeavors, we plan to undertake a more thorough and comprehensive validation of the LWST retrieval outcomes to holistically assess the accuracy and reliability of the cross-calibration methodology. Despite our choice of this approach to achieve completeness in brightness temperature data, we acknowledge the potential for introducing a certain level of uncertainty in any data processing method when applied practically. Hence, we advocate for future investigations to delve deeper into refining and optimizing the cross-calibration method to enhance the precision and credibility of LWST retrieval outcomes.

In future research endeavors, we aim to explore more effective radiometric calibration methods and compensatory strategies to address the influence of wind and temperature drift on the TIR camera's stability during high-altitude flights. This effort is crucial in ensuring the acquisition of accurate and reliable TIR data, thereby providing a more robust foundation for water body monitoring and land surface temperature analysis.

Furthermore, this study utilized only a single set of UAV images. Subsequent research could involve contrasting experiments across different time periods and diverse climatic conditions to refine the p-LWST retrieval method. Such comparative experiments would en-

able a more comprehensive attribution analysis of LWST changes from various perspectives and dimensions, thereby offering deeper insights for subsequent monitoring endeavors.

Given the variations in results captured by the UAV's TIR camera at different observation angles for the same location, we propose comparing two approaches: temperature retrieval from individual TIR images before stitching and temperature retrieval after image stitching. Such a comparative analysis might effectively enhance the precision of LWST retrieval. Future investigations could delve into an in-depth comparison between these two approaches to determine the optimal data processing strategy.

During the process of image stitching, especially for images near the center of the lake, we encountered challenges in extracting water features. This may have arisen due to inadequate flight path configurations. Therefore, we recommend future studies meticulously consider flight path planning to ensure the acquisition of a more representative set of images, particularly in the areas concerning water bodies. To enhance the accuracy of water body image stitching, improved image acquisition techniques or alternative UAV image stitching algorithms could be considered. Additionally, placing floating objects or markers within the lake may augment its capability to capture water features. Potential enhancements also involve the utilization of multispectral or hyperspectral sensors to gather more comprehensive information about the texture and composition of water bodies, facilitating a more thorough reconstruction of the actual conditions within these areas.

Due to the complexity of internal lake structures, such as hydrological variations that may exist in the central lake region, we suggest further exploration in future studies regarding variations in the emissivity of water bodies in these central locations. This exploration aims to provide a comprehensive understanding of the optical characteristics of lakes. Categorizing lakes into different water types and conducting in-depth investigations into their internal composition and optical properties would contribute to improving the accuracy and reliability of LWST.

In addition, our study was confined to the lakeshore area. Despite the broad field of view around the study area, we were constrained by local regulations regarding the maximum flight altitude for UAVs. Despite the limitations on flight duration and legal constraints, UAVs still hold an unparalleled advantage in collecting distributed, high spatial resolution temperature data compared to satellites. Furthermore, in contrast to satellite data limited to daily to weekly scales of monitoring, UAVs can fly on-demand, capturing temperature changes in sensitive areas around the clock.

Overall, through cross-calibration and retrieval analysis of multisource remote sensing data, we successfully revealed the spatiotemporal distribution characteristics of LWST in the study area and made preliminary discussions on its changing trends. This study provides crucial references and foundations for a deeper understanding of the thermodynamics of water bodies in this region. We believe these findings will have a positive impact on related research and aspects such as water resource management.

Finally, this paper emphasizes the practicality of using UAVs to capture LWST changes at a small spatial scale. The overall lake environment exhibits complexity in spatial distribution that is difficult to capture beyond high-resolution remote sensing technologies. Our findings indicate that UAVs can also serve as valuable tools in assessing changes in other lake parameters, such as chlorophyll-a concentration, water color remote sensing, and more. Therefore, UAV technology holds significant potential in assessing the spatial complexities of ecological and urban environments, remote sensing modeling, and parameter retrieval, among other areas. In future research, we will continue exploring and expanding the application of drone technology in the field of Earth observation.

6. Conclusions

In the current realm of UAV-based Thermal Infrared (TIR) data research, temperature retrieval methods have predominantly focused on flat surfaces and complex terrains, with limited attention dedicated to the specific challenges posed by lake water surface temperature (LWST) retrieval. This study introduces a novel approach (p-LWST) specifically

designed for remotely sensing the water surface temperature of plateau lakes. The methodology leverages TIR image data captured by the DJI Zenmuse H20T, incorporating Lake Water Surface Emissivity (LWSE) measured by the 102F spectrometer and atmospheric parameters simulated by MODTRAN5.2 using ERA5 reanalysis data. The method employs cross-calibration with data acquired from the FLIR T610 infrared thermal imaging camera and the Fluke 51-II contact thermometer, ultimately retrieving LWST through a radiative transfer model.

The study utilized the 102F to randomly determine LWSE within the research area, yielding an emissivity value of $\varepsilon = 0.993$. Calibration of the UAV TIR sensor was conducted using the FLIR T610 and Fluke 51-II, resulting in a cross-calibration correction value of $\delta T_S = 12.82$ K. The final retrieval indicates a spatially varying LWST range for the study area, spanning from 288 K to 295 K.

To validate the accuracy of the p-LWST method, empirical data from the FLIR T610 was employed. The validation results demonstrate a high level of precision in the retrieved LWST, with a Root Mean Square Error (RMSE) of 0.89 K for 20 randomly selected points. This method introduces a valuable approach for LWST monitoring in plateau lakes, providing essential technical support for the ongoing monitoring and analysis of ecosystem changes in these unique environments.

Author Contributions: Writing—original draft preparation and methodology, O.S.; writing—methodology, review and editing, B.-H.T.; writing—methodology and editing, Z.-W.H.; methodology and resources, D.W. and J.-L.Z. All authors have read and agreed to the published version of the manuscript.

Funding: This work was supported in part by the National Natural Science Foundation of China under Grant 42230109, in part by the Yunling Scholar Project of the "Xingdian Talent Support Program" of Yunnan Province under Grant KKRC202221002, and in part by the Platform Construction Project of High Level Talent in the Kunming University of Science and Technology (KUST) under Grant KKZ7202221001.

Institutional Review Board Statement: Not applicable.

Informed Consent Statement: Not applicable.

Data Availability Statement: The ERA 5 data can be obtained from the ECMWF website https://cds.climate.copernicus.eu/ (accessed on 10 November 2023).

Acknowledgments: Thanks to the Forest Fire Brigade of Dali Bai Autonomous Prefecture and the Erhai Lake Management Bureau of Dali Bai Autonomous Prefecture in Yunnan Province, China, for their support in this research.

Conflicts of Interest: The authors declare that they have no known competing financial interests or personal relationships that could have appeared to influence the work reported in this paper.

References

1. Jia, T.F.; Yang, K.; Peng, Z.Q.; Tang, L.F.; Duan, H.M.; Luo, Y. Review on the Change Trend, Attribution Analysis, Retrieval, Simulation, and Prediction of Lake Surface Water Temperature. *IEEE J. Sel. Top. Appl. Earth Obs. Remote Sens.* **2022**, *15*, 6324–6355. [CrossRef]
2. Wang, D.; Tang, B.-H.; Fu, Z.; Huang, L.; Li, M.; Chen, G.; Pan, X. Estimation of Chlorophyll-A Concentration with Remotely Sensed Data for the Nine Plateau Lakes in Yunnan Province. *Remote Sens.* **2022**, *14*, 4950. [CrossRef]
3. Rigosi, A.; Hanson, P.; Hamilton, D.P.; Hipsey, M.; Rusak, J.A.; Bois, J.; Sparber, K.; Chorus, I.; Watkinson, A.J.; Qin, B.Q.; et al. Determining the probability of cyanobacterial blooms: The application of Bayesian networks in multiple lake systems. *Ecol. Appl.* **2015**, *25*, 186–199. [CrossRef] [PubMed]
4. Li, Z.-L.; Tang, B.-H.; Wu, H.; Ren, H.Z.; Yan, G.J.; Wan, Z.M.; Trigo, I.F.; Sobrino, J.A. Satellite-derived land surface temperature: Current status and perspectives. *Remote Sens. Environ.* **2013**, *131*, 14–37. [CrossRef]
5. He, Z.-W.; Tang, B.-H. Retrieval of Rugged Mountainous Areas Land Surface Temperature from High-spatial-resolution Thermal Infrared Remote Sensing Data. *IEEE Trans. Geosci. Remote Sens.* **2023**, *61*, 4508216. [CrossRef]
6. Zhu, X.L.; Duan, S.B.; Li, Z.-L.; Zhao, W.; Wu, H.; Leng, P.; Gao, M.F.; Zhou, X.M. Retrieval of Land Surface Temperature with Topographic Effect Correction from Landsat 8 Thermal Infrared Data in Mountainous Areas. *IEEE Trans. Geosci. Remote Sens.* **2021**, *59*, 6674–6687. [CrossRef]

7. Duan, S.-B.; Li, Z.-L.; Wang, C.; Zhang, S.; Tang, B.-H.; Leng, P.; Gao, M.-F. Land-surface temperature retrieval from Landsat 8 single-channel thermal infrared data in combination with NCEP reanalysis data and ASTER GED product. *Int. J. Remote Sens.* **2019**, *40*, 1763–1778. [CrossRef]
8. Tang, B.-H.; Bi, Y.Y.; Li, Z.-L.; Xia, J. Generalized Split-Window algorithm for estimate of Land Surface Temperature from Chinese geostationary FengYun meteorological satellite (FY-2C) data. *Sensors* **2008**, *8*, 933–951. [CrossRef]
9. Wang, L.J.; Guo, N.; Wang, W.; Zuo, H.C. Optimization of the Local Split-Window Algorithm for FY-4A Land Surface Temperature Retrieval. *Remote Sens.* **2019**, *11*, 2016. [CrossRef]
10. Ye, X.; Ren, H.Z.; Zhu, J.S.; Fan, W.J.; Qin, Q.M. Split-Window Algorithm for Land Surface Temperature Retrieval from Landsat-9 Remote Sensing Images. *IEEE Geosci. Remote Sens. Lett.* **2022**, *19*, 7507205. [CrossRef]
11. Ye, X.; Ren, H.Z.; Zhu, J.S.; Zeng, H.; Wang, B.Z.; Huang, H.; Fan, W.J. Land Surface Temperature Retrieval Based on Thermal Infrared Channel Decomposed Split-Window Algorithm. *IEEE J. Sel. Top. Appl. Earth Obs. Remote Sens.* **2022**, *15*, 4971–4979. [CrossRef]
12. Tang, B.-H.; Wang, J. A Physics-Based Method to Retrieve Land Surface Temperature from MODIS Daytime Midinfrared Data. *IEEE Trans. Geosci. Remote Sens.* **2016**, *54*, 4672–4679. [CrossRef]
13. Tang, B.-H. Nonlinear Split-Window Algorithms for Estimating Land and Sea Surface Temperatures from Simulated Chinese Gaofen-5 Satellite Data. *IEEE Trans. Geosci. Remote Sens.* **2018**, *56*, 6280–6289. [CrossRef]
14. Gillespie, A.; Rokugawa, S.; Matsunaga, T.; Cothern, J.S.; Hook, S.; Kahle, A.B. A temperature and emissivity separation algorithm for Advanced Spaceborne Thermal Emission and Reflection Radiometer (ASTER) images. *IEEE Trans. Geosci. Remote Sens.* **1998**, *36*, 1113–1126. [CrossRef]
15. Liu, W.H.; Shi, J.C.; Liang, S.L.; Zhou, S.G.; Cheng, J. Simultaneous retrieval of land surface temperature and emissivity from the FengYun-4A advanced geosynchronous radiance imager. *Int. J. Digit. Earth* **2022**, *15*, 198–225. [CrossRef]
16. Wan, Z.; Li, Z.-L. A physics-based algorithm for retrieving land-surface emissivity and temperature from EOS/MODIS data. *IEEE Trans. Geosci. Remote Sens.* **1997**, *35*, 980–996. [CrossRef]
17. Coll, C.; Caselles, V.; Galve, J.M.; Valor, E.; Niclòs, R.; Sánchez, J.M. Evaluation of split-window and dual-angle correction methods for land surface temperature retrieval from Envisat/Advanced Along Track Scanning Radiometer (AATSR). *J. Geophys. Res.* **2006**, *111*, D12105. [CrossRef]
18. Li, Z.-L.; Wu, H.; Duan, S.-B.; Zhao, W.; Ren, H.; Liu, X.; Leng, P.; Tang, R.; Ye, X.; Zhu, J.; et al. Satellite Remote Sensing of Global Land Surface Temperature: Definition, Methods, Products, and Applications. *Rev. Geophys.* **2023**, *61*, e2022RG000777. [CrossRef]
19. Zhao, Y.S.; Yang, K.; Luo, Y.; Yu, Z.Y. Spatial-temporal characteristics of surface thermal environment and its effect on Lake surface water temperature in Dianchi Lake basin. *Front. Ecol. Evol.* **2022**, *10*, 984692. [CrossRef]
20. Wang, Z.W.; Zhou, J.; Liu, S.M.; Li, M.S.; Zhang, X.D.; Huang, Z.M.; Dong, W.C.; Ma, J.; Ai, L.J. A Land Surface Temperature Retrieval Method for UAV Broadband Thermal Imager Data. *IEEE Geosci. Remote Sens. Lett.* **2022**, *19*, 7002805. [CrossRef]
21. Song, B.; Park, K. Verification of Accuracy of Unmanned Aerial Vehicle (UAV) Land Surface Temperature Images Using In-Situ Data. *Remote Sens.* **2020**, *12*, 288. [CrossRef]
22. Kelly, J.; Kljun, N.; Olsson, P.-O.; Mihai, L.; Liljeblad, B.; Weslien, P.; Klemedtsson, L.; Eklundh, L. Challenges and Best Practices for Deriving Temperature Data from an Uncalibrated UAV Thermal Infrared Camera. *Remote Sens.* **2019**, *11*, 567. [CrossRef]
23. Kim, D.; Yu, J.; Yoon, J.; Jeon, S.; Son, S. Comparison of Accuracy of Surface Temperature Images from Unmanned Aerial Vehicle and Satellite for Precise Thermal Environment Monitoring of Urban Parks Using in Situ Data. *Remote Sens.* **2021**, *13*, 1977. [CrossRef]
24. Awais, M.; Li, W.; Hussain, S.; Cheema, M.J.M.; Li, W.; Song, R.; Liu, C. Comparative Evaluation of Land Surface Temperature Images from Unmanned Aerial Vehicle and Satellite Observation for Agricultural Areas Using In Situ Data. *Agriculture* **2022**, *12*, 184. [CrossRef]
25. Naughton, J.; McDonald, W. Evaluating the Variability of Urban Land Surface Temperatures Using Drone Observations. *Remote Sens.* **2019**, *11*, 1722. [CrossRef]
26. Heinemann, S.; Siegmann, B.; Thonfeld, F.; Muro, J.; Jedmowski, C.; Kemna, A.; Kraska, T.; Muller, O.; Schultz, J.; Udelhoven, T.; et al. Land Surface Temperature Retrieval for Agricultural Areas Using a Novel UAV Platform Equipped with a Thermal Infrared and Multispectral Sensor. *Remote Sens.* **2020**, *12*, 1075. [CrossRef]
27. Xu, S.S.; Yang, K.; Xu, Y.T.; Zhu, Y.H.; Luo, Y.; Shang, C.X.; Zhang, J.; Zhang, Y.; Gao, M.; Wu, C.H. Urban Land Surface Temperature Monitoring and Surface Thermal Runoff Pollution Evaluation Using UAV Thermal Remote Sensing Technology. *Sustainability* **2021**, *13*, 1203. [CrossRef]
28. Berk, A.; Anderson, G.; Acharya, P.; Shettle, E. *MODTRAN 5.2. 2 User's Manual Spectral Sciences*; Spectral Sciences Inc.: Burlington, MA, USA, 2011; p. 69.
29. Wang, Z.; Zhou, J.; Ma, J.; Wang, Y.; Liu, S.; Ding, L.; Tang, W.; Pakezhamu, N.; Meng, L. Removing temperature drift and temporal variation in thermal infrared images of a UAV uncooled thermal infrared imager. *ISPRS J. Photogramm. Remote Sens.* **2023**, *203*, 392–411. [CrossRef]